Supplementary Information

Structural modulation in potassium birnessite single crystals

Liliia D. Kulish,* Pavan Nukala, Rick Scholtens, A. G. Mike Uiterwijk, Ruben Hamming-Green and Graeme R. Blake

Table of contents

1. Composition and structure of K-bir synthesized with $KNO_3 – B_2O_3$ flux and Pt crucible (Sample 2)

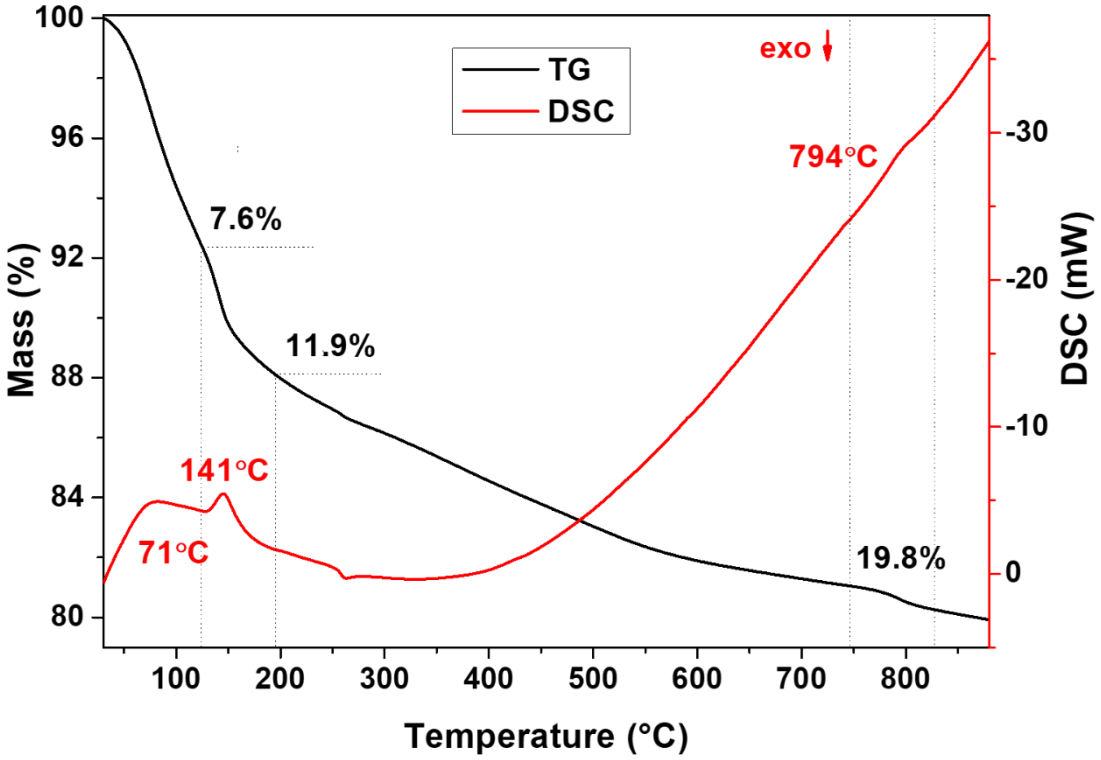

Fig. S1 Thermal analysis of potassium birnessite (sample 2). The TG and DSC data are represented by the black and red lines respectively. The lowest temperature feature corresponds to surface water evaporation with a mass loss of 7.6 % and a maximum in the DSC curve at 71 °C. The second endothermal effect with the sharp maximum in the DSC curve at 141 °C corresponds to the release of interlayer crystal water with a further mass loss of 4.3 %. The third endothermal effect with a maximum in the DSC curve at 794 °C can be attributed to the formation of high-temperature manganese oxide polymorphs.

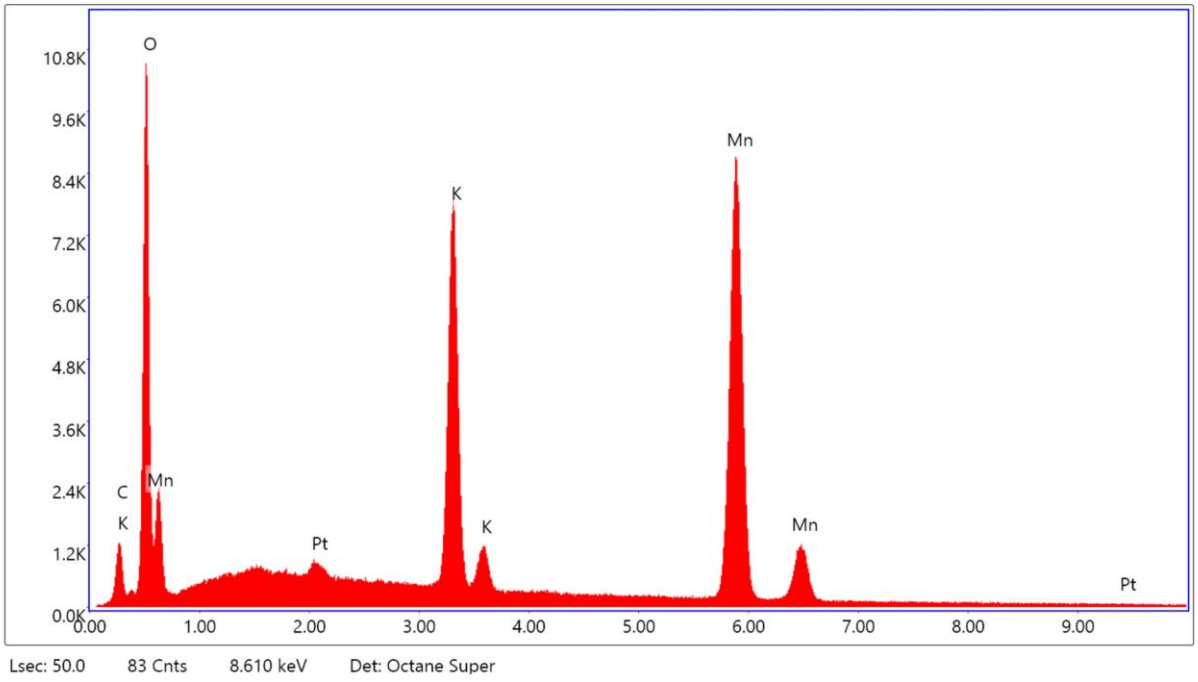

Fig. S2 EDS spectrum of potassium birnessite (sample 2).

Table S1 EDS atomic percentages of the elements in potassium birnessite (sample 2). The presence of a small amount of platinum is from the crucible. Pt is randomly distributed over the whole volume.

Element	Weight %	Atomic %	Error %
O K	19.2	43.2	7.8
Pt M	1.1	0.2	12.9
K K	16.1	14.8	2.6
Mn K	63.7	41.8	2.5

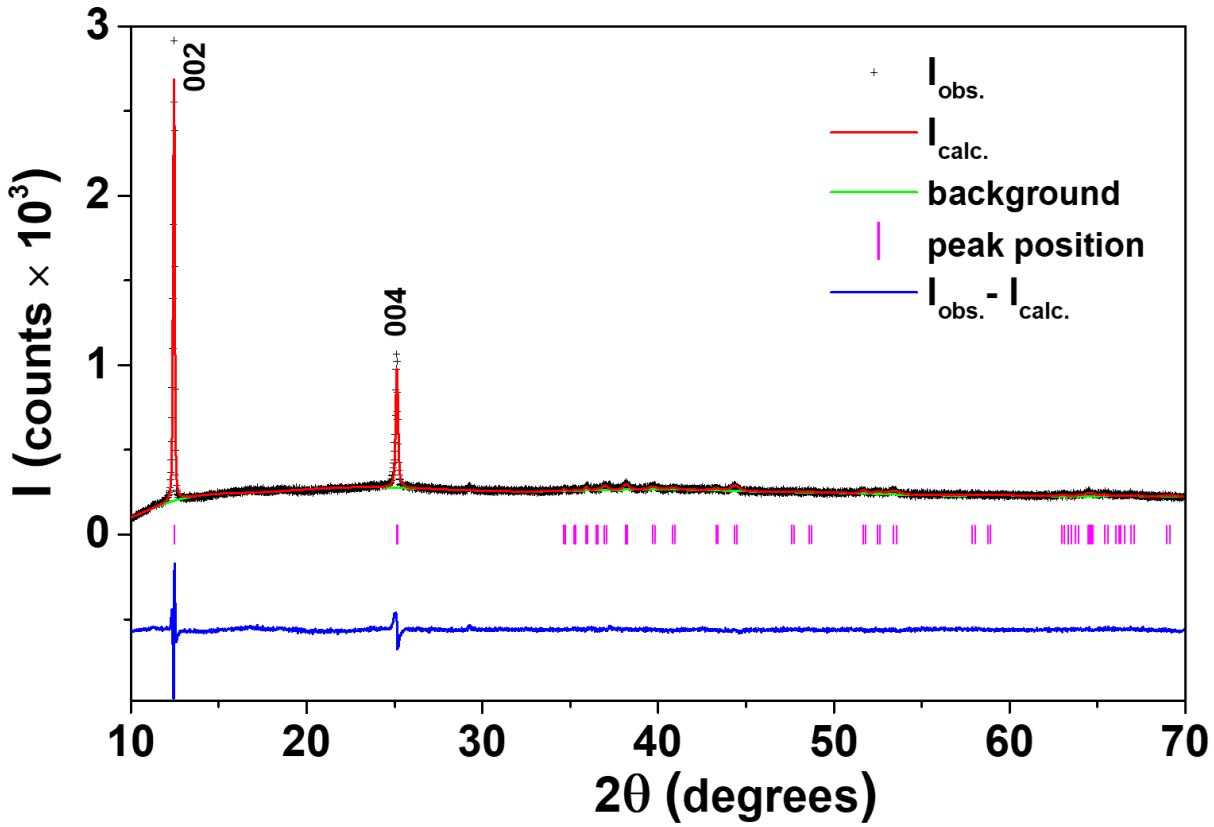

Fig. S3 Fitted powder XRD data of potassium birnessite (sample 2). The observed data are denoted by black crosses, the calculated profile is the red line, and the difference profile is the lower blue line. The pink markers indicate the positions of allowed Bragg peaks. The peak intensities could only be fitted well when a preferential orientation model was included in the fitting, accounting for a preferred packing of crystallites along the [001] direction.

Table S2 Composition and structural parameters of potassium birnessite (sample 2). The potassium-manganese ratio of K : Mn = 0.36 : 1 and the percentage mass loss of crystal water determined during heating of the sample gave an average composition of $K_{0.36}MnO_2 \cdot 0.25H_2O$.

Compound	Space Group	*a*	*b*	*c*	α = β = γ	Volume
$K_{0.36}MnO_2 \cdot 0.25H_2O$	*Cmcm*	2.8493(11) Å	5.168(3) Å	14.1270(3) Å	90°	208.00(13) Å^3

2. Composition and structure of Sample 3 synthesized using PbO – B_2O_3 flux and Pt crucible

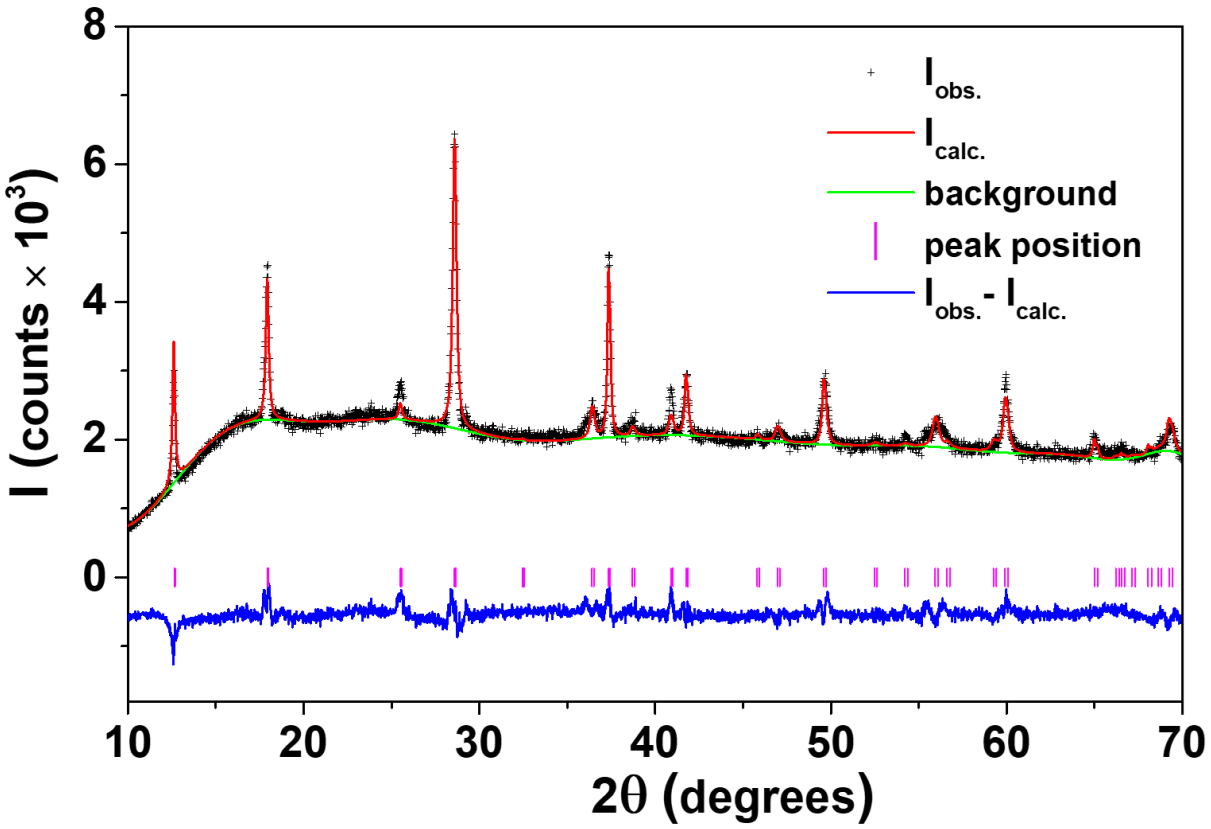

Fig. S4 Fitted powder XRD data for cryptomelane phase KMn_8O_{16} (sample 3). The observed data are denoted by black crosses, the calculated profile is the red line, and the difference profile is the lower blue line. The pink markers indicate the positions of allowed Bragg peaks.

Table S3 Composition and structural parameters of cryptomelane phase (sample 3).

Compound	Space Group	*a*	*b*	*c*	α = β = γ	Volume
KMn_8O_{16}	*I4/m*	9.8461(5) Å	9.8461(5) Å	2.8653(2) Å	90°	277.78(3) Å^3

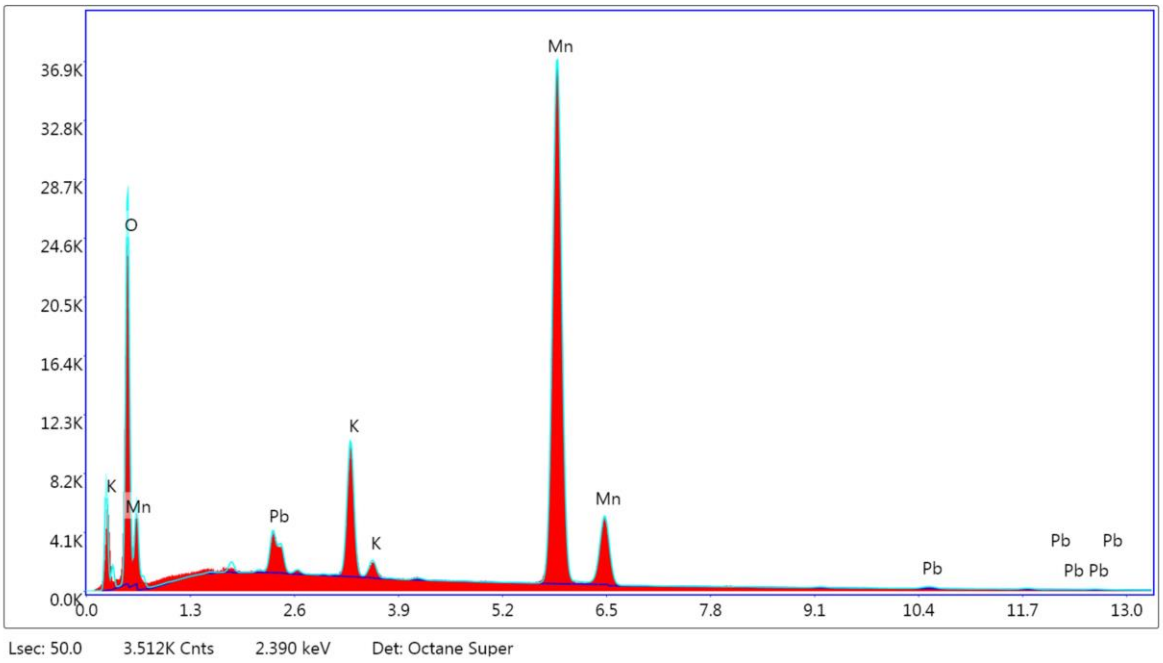

Fig. S5 EDS spectrum of cryptomelane (sample 3).

Table S4 EDS atomic percentages of the elements in cryptomelane (sample 3). The presence of a small amount of lead is from the flux. Pb is equally distributed over the whole volume.

Element	Weight %	Atomic %	Error %
O K	20.9	47.5	7.1
Pb M	3.5	0.6	6.5
K K	6.6	6.2	2.6
Mn K	69.0	45.7	1.6

3. Uniformity of $K_{0.31}MnO_2 \cdot 0.41H_2O$ composition (Sample 1)

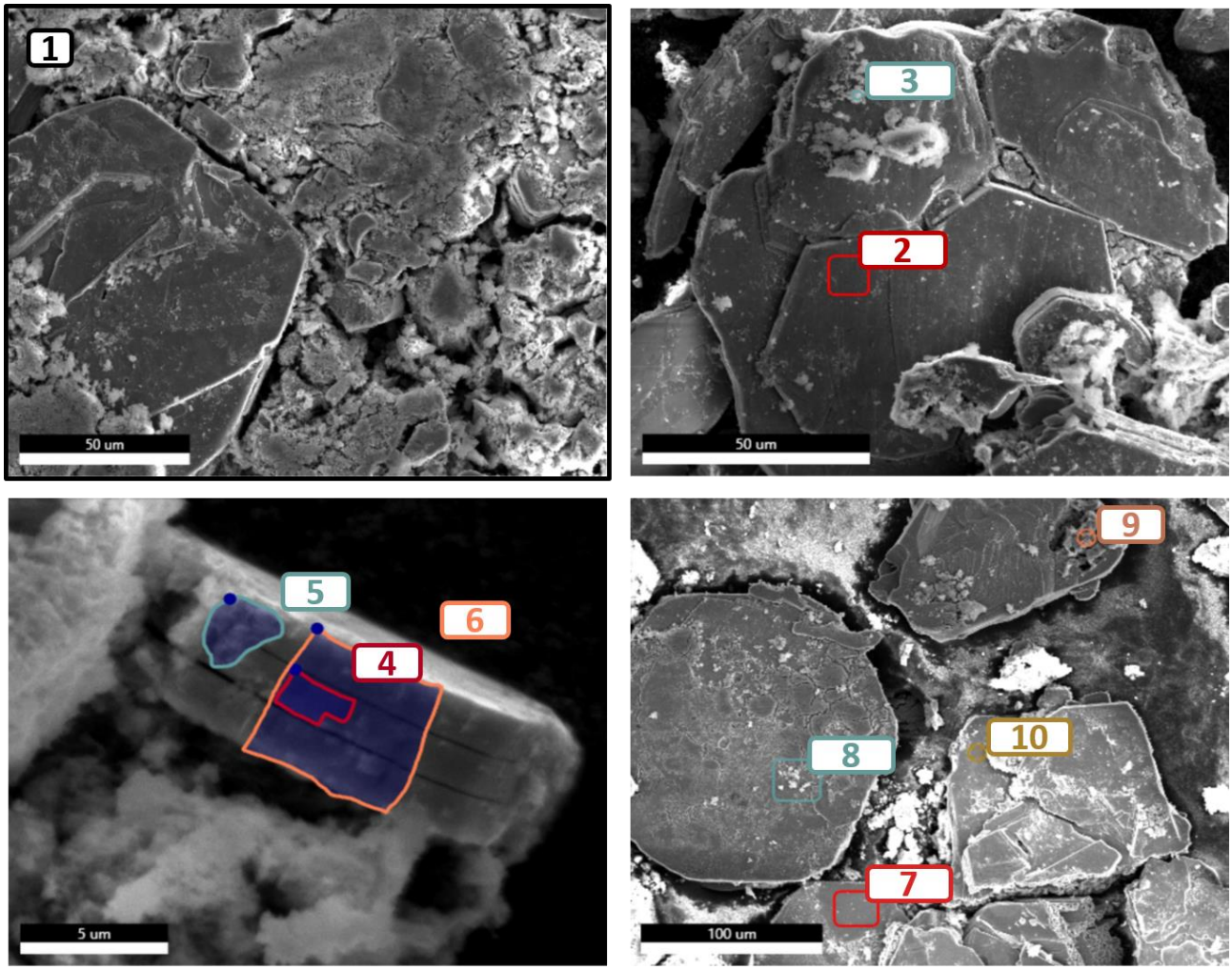

Fig. S6 SEM images of $K_{0.31}MnO_2 \cdot 0.41H_2O$ (sample 1). Numbers show areas 1 – 10 where EDS measurements were performed.

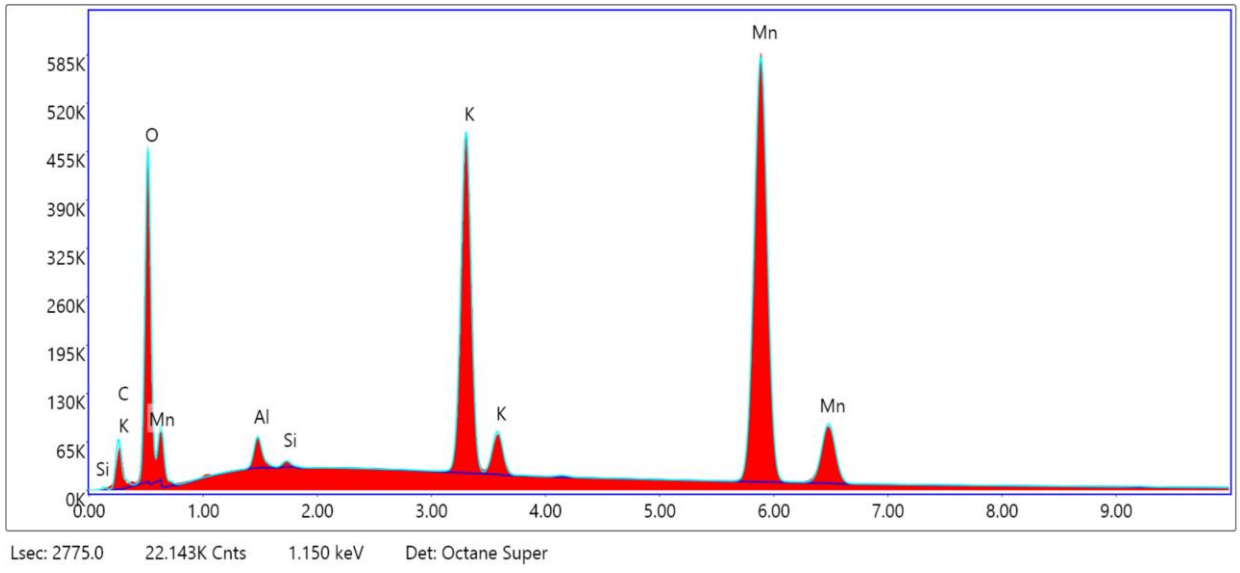

Fig. S7 EDS spectrum of area 1 in Fig. S6.

Table S5 EDS atomic percentages of the elements in areas 1 – 10 in Fig. S6.

No Area	Element	Weight %	Atomic %	Error %
1	O K	13.08	30.20	7.52
	Al M	0.84	1.16	6.11
	K K	15.22	14.38	2.10
	Mn K	67.97	45.69	2.17
2	O K	21.17	45.86	7.33
	Al M	1.15	1.48	8.13
	K K	14.33	12.70	2.40
	Mn K	63.35	39.97	2.35
3	O K	23.46	49.03	7.49
	Al M	0.88	1.09	10.15
	K K	14.91	12.75	2.53
	Mn K	60.49	36.82	2.47
4	O K	15.98	37.61	7.65
	Al M	0.87	1.21	10.10
	K K	14.91	14.36	2.61
	Mn K	68.19	46.74	2.47
5	O K	13.88	33.95	7.65
	Al M	0.62	0.90	11.69
	K K	14.32	14.33	2.67
	Mn K	70.98	50.55	2.46
6	O K	15.45	36.67	7.68
	Al M	0.90	1.27	9.71
	K K	14.99	14.56	2.58
	Mn K	68.56	47.38	2.47
7	O K	19.92	44.03	7.56
	Al M	0.72	0.94	11.13
	K K	14.92	13.49	2.55
	Mn K	64.34	41.41	2.47
8	O K	15.93	37.53	7.68
	Al M	0.78	1.09	10.48
	K K	15.13	14.58	2.57
	Mn K	68.09	46.71	2.46
9	O K	19.11	42.97	7.14
	Al M	0.88	1.17	9.86
	K K	11.48	10.56	2.72
	Mn K	67.83	44.40	2.44
10	O K	22.27	47.42	7.26
	Al M	1.60	2.02	8.13
	K K	12.89	11.23	2.63
	Mn K	63.05	39.10	2.45

Table S6 Data from EDS atomic percentages of the elements used to calculate the average K/Mn ratio of sample 1, and error propagation of the ratio.

The following equations were used:

$$\boldsymbol{\Delta R} = \frac{\mathbf{1}}{\boldsymbol{\chi_{Mn}}} \times \sqrt{\Delta\boldsymbol{\chi_K^2} + \boldsymbol{R_{K/Mn}^2} \times \Delta\boldsymbol{\chi_{Mn}^2}}$$

$$\boldsymbol{\Delta R_{avg}} = \frac{\mathbf{1}}{\boldsymbol{A_1 + \cdots + A_{10}}} \times \sqrt{\boldsymbol{A_1^2} \times \Delta\mathbf{R_1^2} + \cdots + \boldsymbol{A_{10}^2} \times \Delta\mathbf{R_{10}^2}}$$

Here, ΔR is the propagated error for element ratio $R_{K/Mn}$; χ_{Mn} is the atomic percentage of Mn in a given area; $\Delta\chi$ is the uncertainty in the EDS measurement for K or Mn; ΔR_{avg} is the propagated error for the average ratio R_{avg}; A is the area of the EDS measurement.

No	A, μm^2	χ_K,%	$\Delta\chi_K$,%	χ_{Mn},%	$\Delta\chi_{Mn}$,%	$R_{K/Mn}$	$R_{avg\ K/Mn}$	ΔR	ΔR_{avg}
1	23779.6	14.38	0.30	45.69	0.99	0.31	0.30	0.01	0.01
2	78.0	12.90	0.31	40.62	0.95	0.32		0.01	
3	2.5	12.94	0.33	37.40	0.92	0.35		0.01	
4	2.6	14.54	0.38	47.39	1.17	0.31		0.01	
5	9.4	14.50	0.39	51.19	1.26	0.28		0.01	
6	24.0	14.76	0.38	48.09	1.19	0.31		0.01	
7	439.9	13.63	0.35	42.03	1.04	0.32		0.01	
8	580.7	14.76	0.38	47.27	1.16	0.31		0.01	
9	11.0	10.81	0.30	45.74	1.11	0.24		0.01	
10	11.0	11.51	0.30	40.45	0.99	0.28		0.01	

4. XPS spectrum of $K_{0.31}MnO_2 \cdot 0.41H_2O$ (Sample 1)

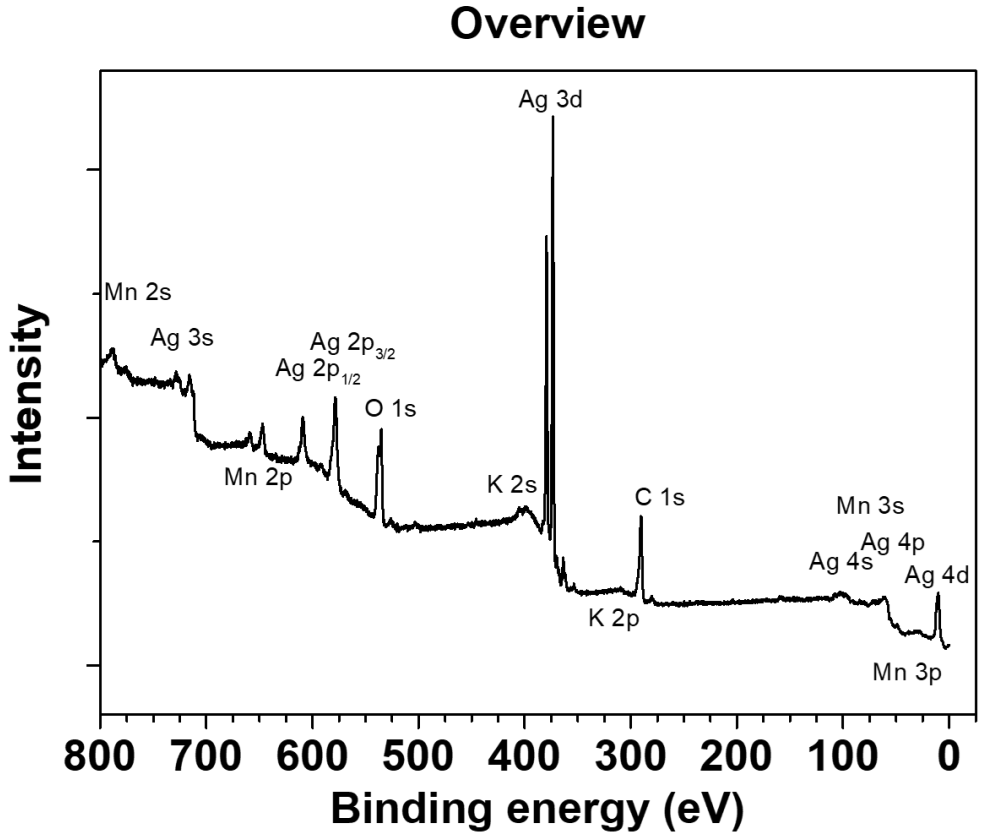

Fig. S8 XPS spectrum of K-bir (sample 1). The overview shows the presence of Mn, O, K in the sample. The Ag signal is from the silver paste used for preparing the sample, carbon is from the atmosphere.

5. Structural parameters of $K_{0.31}MnO_2 \cdot 0.41H_2O$ from SC XRD data (Sample 1)

Table S7 Crystallographic and refinement parameters of K-bir (sample 1).

Temperature (K)	100(2)
Crystal size (mm^3)	0.16 × 0.12 × 0.02
Crystal color	Dark brown
Crystal system	orthorhombic
Space group	*Cmcm* (no. 63)
Z	4
D (calculated) (g/cm3)	3.444
F(000)	201
a (Å)	2.897(4)
b (Å)	4.980(9)
c (Å)	14.12(2)
α = β = γ (°)	90
Volume ($Å^3$)	203.6(6)
μ (mm^{-1})	6.726
Min/max transmission	0.5072/0.7461
θ range (degrees)	2.886-28.253
Index ranges	−3 < h < 3 −6 < k < 6 −18 < l < 18
Data/restraints/parameters	165/0/13
GooF of F^2	1.445
No. total reflections	2579
No. unique reflections	165
No. obs Fo > 4σ(Fo)	148
R_1 [Fo > 4σ(Fo)]	0.0759
R_1 [all data]	0.0863
wR_2 [Fo > 4σ(Fo)]	0.2019
wR_2 [all data]	0.1924
Largest peak and hole (e $Å^3$)	1.638 and -1.073

Table S8 Refined Mn-O bond lengths and Mn-O-Mn angles in K-bir (sample 1).

	Bond length (Å)		Bond angle (°)
Mn-O	1.921(12) × 2	Mn-O-Mn	96.7(3)
Mn-O	1.934(7) × 4	Mn-O-Mn	96.7(3)
		Mn-O-Mn	97.0(5)

6. Modulation of the layered structure of $K_{0.31}MnO_2 \cdot 0.41H_2O$ (Sample 1)

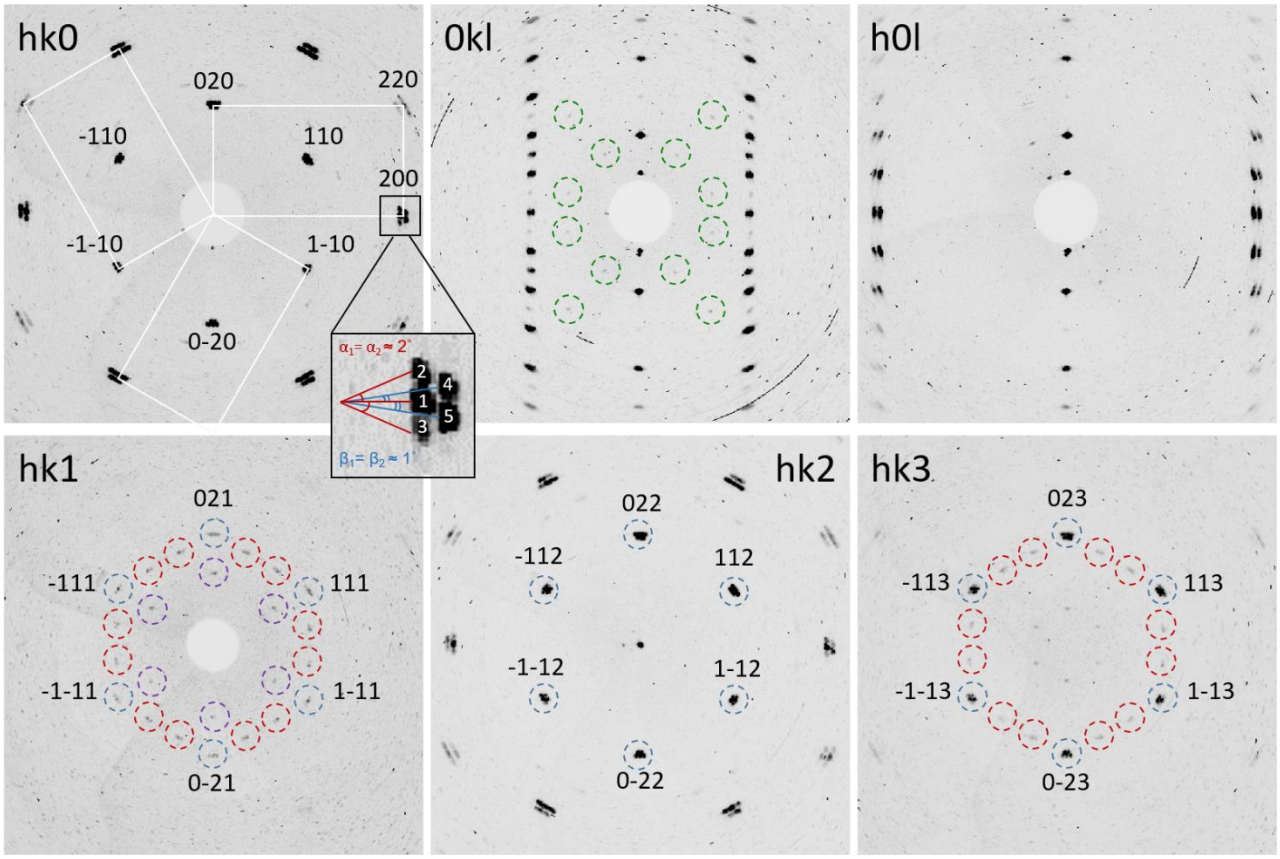

Fig. S9 Precession images of different reciprocal lattice planes generated from raw SC XRD data of K-bir (sample 1).

Each cluster consists of rows of three and two spots (labelled 1-3 and 4-5 respectively). The first possible explanation to consider is the presence of five different orthorhombic domains. In this interpretation, domains 1, 2 and 3 have the same lattice parameters ($a \approx 2.85$, $b \approx 5.00$, $c \approx 14.13$ Å) and differ from each other by a rotation of approximately ± 2 degrees of domains 2 and 3 with respect to the middle domain 1 around the reciprocal *c*-axis. Domains 4 and 5 are rotated by approximately ± 1 degree from the middle domain 1, but they have larger *a* and *b* lattice parameters ($a \approx 2.93$, $b \approx 5.15$, $c \approx 14.13$ Å). In addition, for an orthorhombic distortion of a hexagonal structure as is the case here, we expect three orthorhombic domains that are rotated by 120 degrees in the basal plane (shown as white rectangles in Fig. S9, *hk0* plane). The result would be the superposition of spots from 15 domains at each cluster position. However, close inspection of the cluster pattern allows us to rule out this multi-domain explanation for the clusters. For example, clusters *020* and *200* have three outer and two inner spots, but cluster *200* which lies on the same rectangle (the same rotational domain) has two inner spots and three outer spots. Therefore, consistent indexing of the spots within clusters cannot be achieved using this model. Furthermore, powder XRD shows the existence of only one phase (Fig. S10 and Fig. S11); the difference in lattice parameters between domains 1-3 and 4-5 would be visible as split peaks.

Close inspection of the raw XRD data reveals signatures of an in-plane structural modulation, such as the additional weak spots in the reciprocal *0kl* plane (indicated by open green circles in Fig. S9, further details in Fig. S12). These superlattice spots suggest an approximate tripling of the unit cell in the *b*-direction. The planes *hk1* and *hk3* also contain extra spots with non-integer values of both *h* and *k*, implying that the modulation occurs along the pseudo-hexagonal axes. The extra spots also form clusters, thus the clustering likely originates from another, incommensurate modulation with a long period resulting in spots that are close together in reciprocal space.

7. Powder XRD data of $K_{0.31}MnO_2 \cdot 0.41H_2O$ (Sample 1)

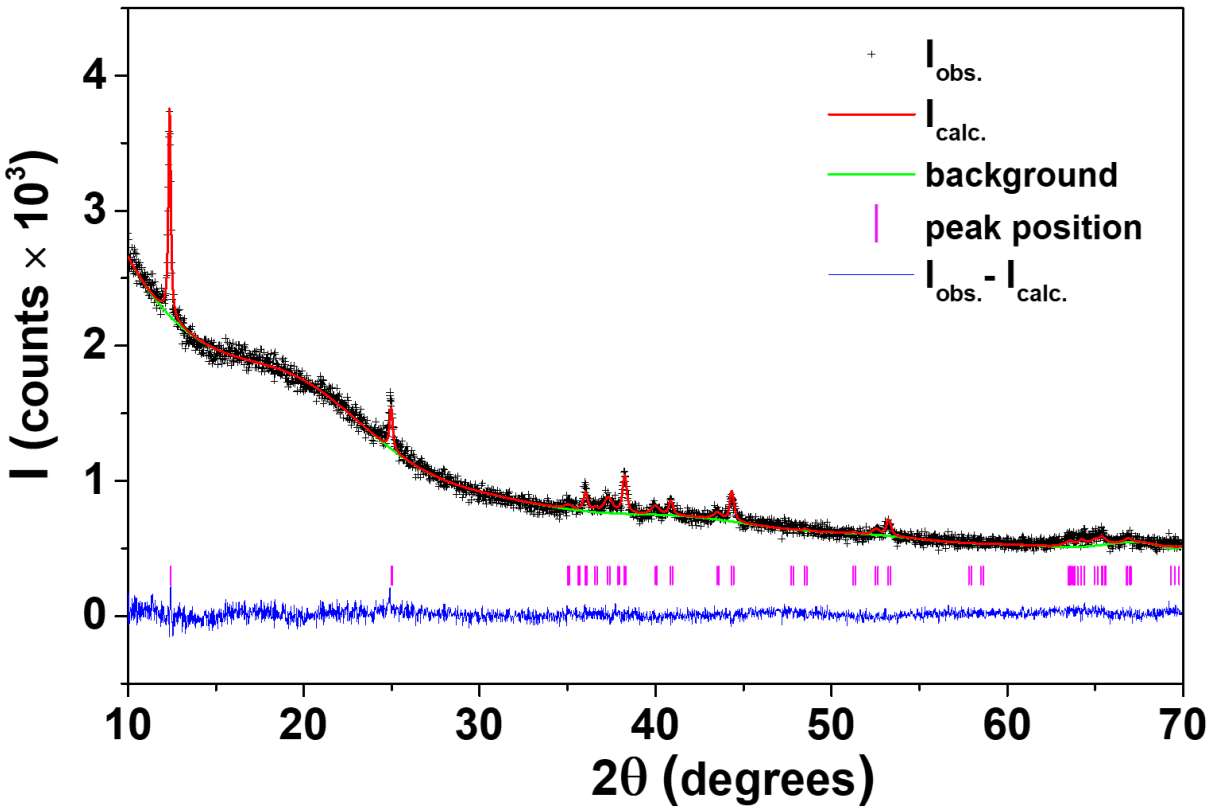

Fig. S10 Fitted powder XRD data for $K_{0.31}MnO_2 \cdot 0.41H_2O$ (sample 1). The observed data are denoted by black crosses, the calculated profile is the red line, and the difference profile is the lower blue line. The pink markers indicate the positions of allowed Bragg peaks. K-bir has a preferred packing orientation of the crystallites. For minimization of the preferred orientation, transmission geometry was used. The ground sample (obtained single crystals and powder) was placed on transparent sticky tape in a flat rotating sample holder. The broad maximum at 15-20 ° is from the tape.

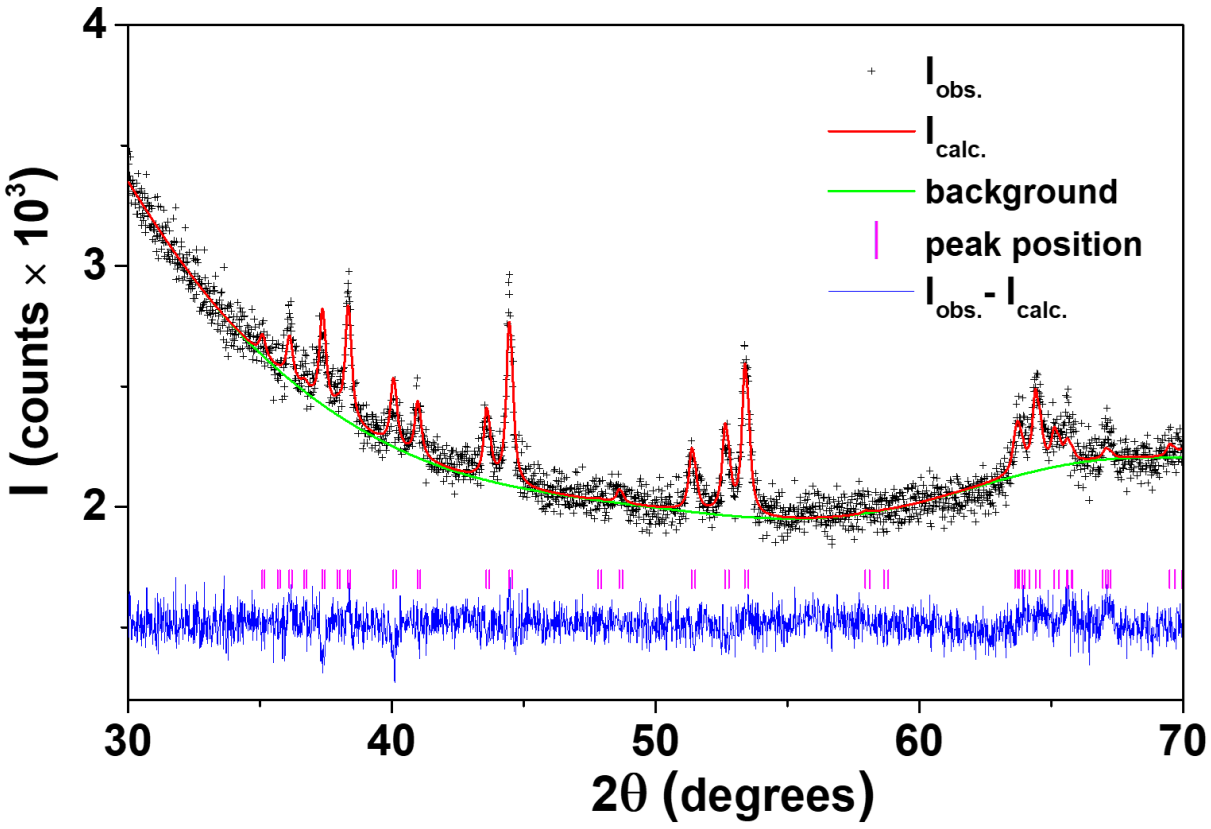

Fig. S11 Fitted powder XRD pattern of additional measurement in the range 2θ = 30-70° (sample 1). The observed data are denoted by black crosses, the calculated profile is the red line, and the difference profile is the lower blue line. The pink markers indicate the positions of allowed Bragg peaks. A rotating glass capillary (d = 0.5 mm) containing the sample was used in transmission geometry. The XRD data confirm a single-phase product.

Table S9 Structural parameters of $K_{0.31}MnO_2 \cdot 0.41H_2O$ (sample 1) from powder XRD at room temperature. The obtained lattice parameters are consistent with those from the single-crystal XRD data at 100 K if thermal expansion of the sample is taken into account.

Compound	Space Group	*a*	*b*	*c*	α = β = γ	Volume
$K_{0.31}MnO_2 \cdot 0.41H_2O$	*Cmcm*	2.8529(6) Å	5.120(2) Å	14.255(2) Å	90°	208.22(8) Å^3

8. Additional modulation of structure and charge-ordered nanodomains in $K_{0.31}MnO_2 \cdot 0.41H_2O$ (Sample 1)

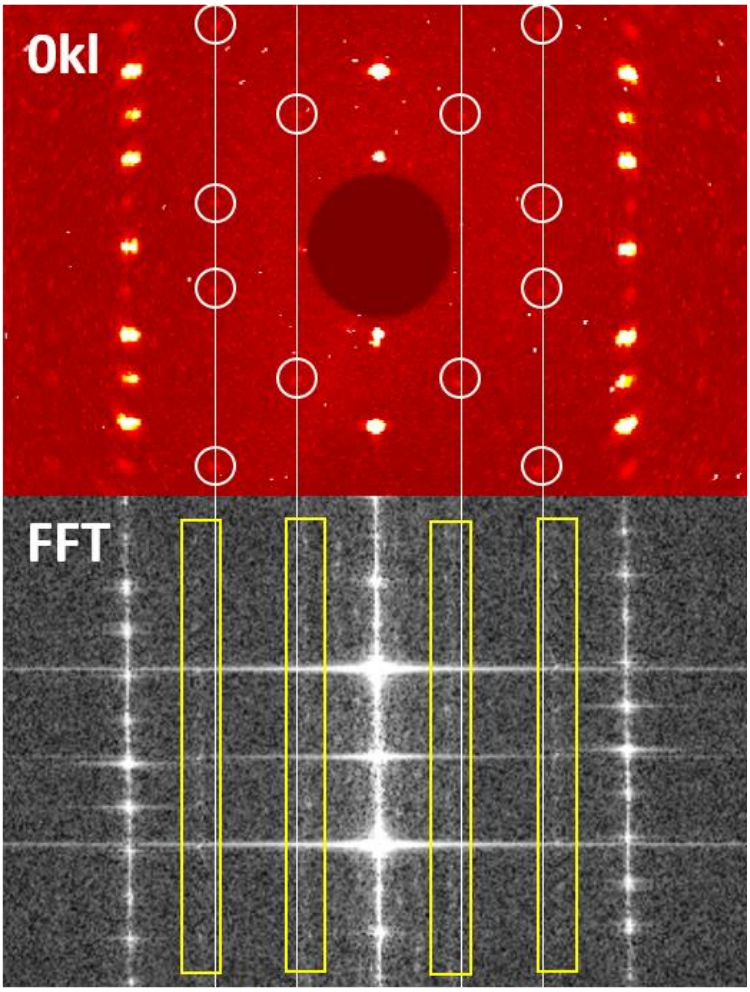

Fig. S12 Comparison of *0kl* plane synthesized from raw SC XRD data (collected at 100 K) and FFT of HAADF-STEM image of the same *0kl* plane (measured at room temperature). The open circles show additional weak spots at non-integer *k*-values. White lines connect spots with non-integer *k*-indices in the reciprocal *c*-direction and do not exactly coincide with the positions of equivalent spots in the FFT image, indicated by yellow rectangles. These spots might be a result of temperature-dependent modulation.

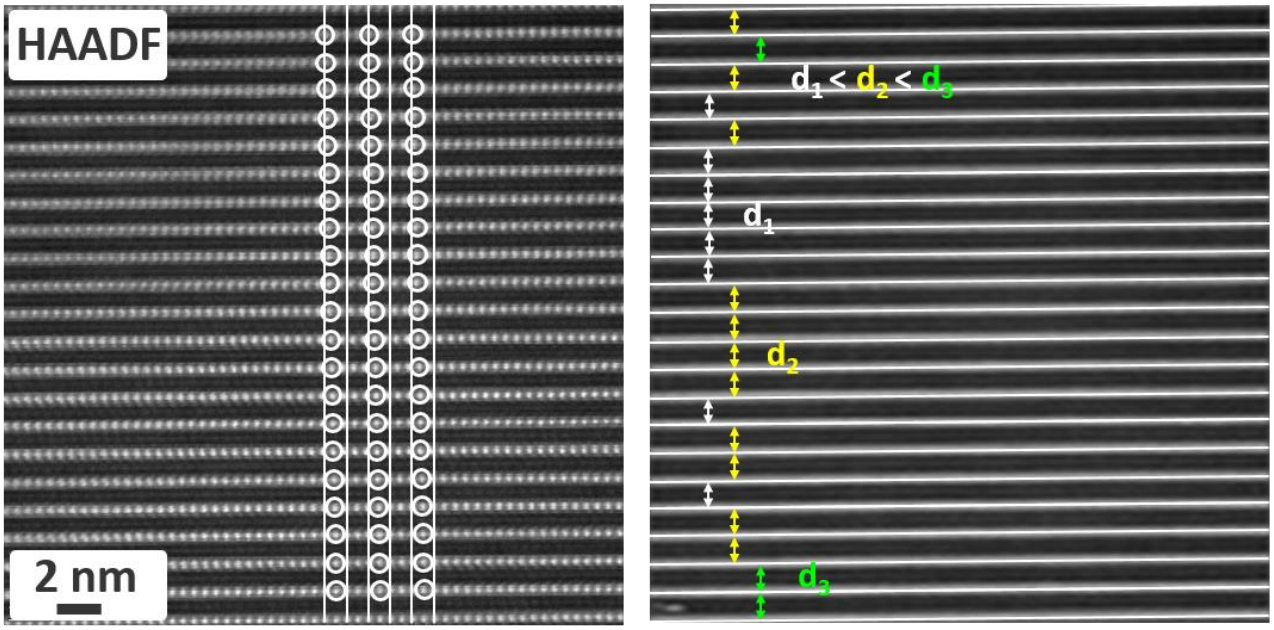

Fig. S13 HAADF-STEM image of a region with stacking fault (left) and Fourier-filtered image with only the *c*-planes (right) showing three different inter-layer spacings associated with stacking disorder. The white lines connect the equivalent points in each layer, the white circles show the positions of MnO_6 octahedra.

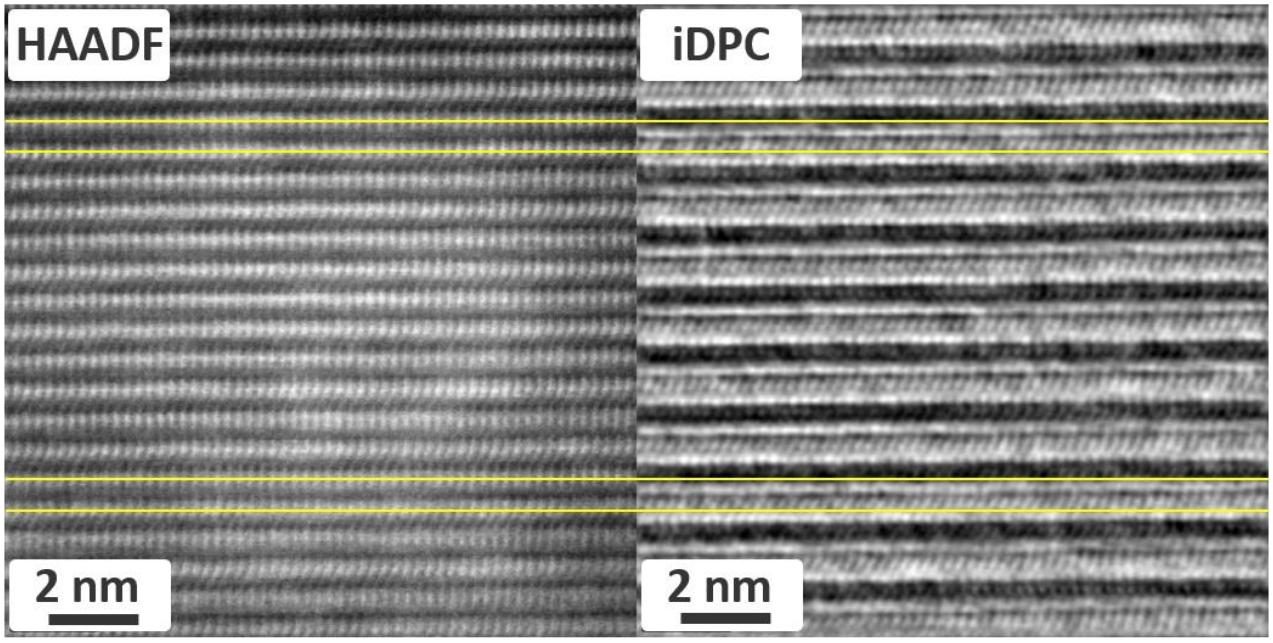

Fig. S14 iDPC-STEM image (right) of another nanodomain shows different alternating contrast of the MnO_6 planes to that in Fig. 8, which is not seen in the HAADF-STEM image (left). Yellow lines connect the equivalent layers.

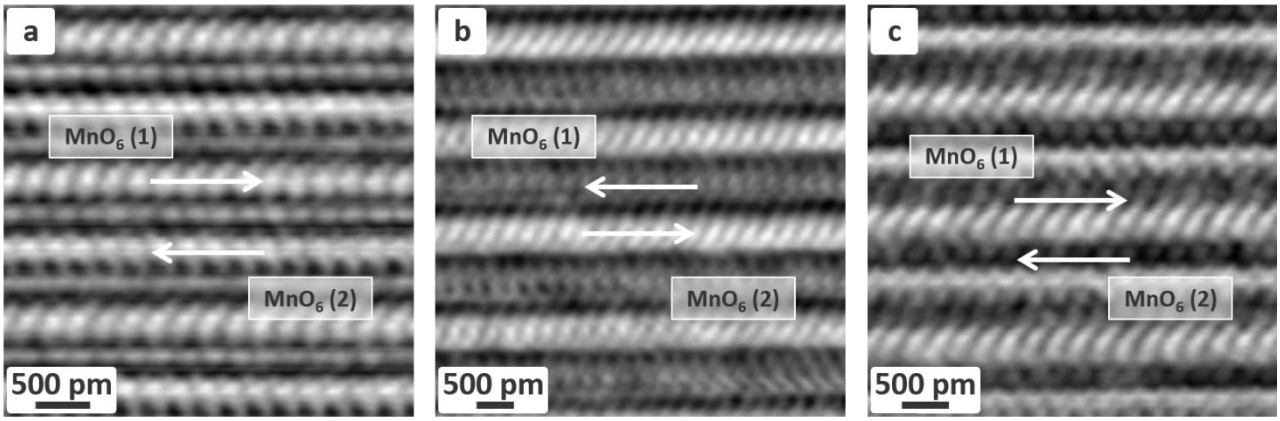

Fig. S15 iDPC-STEM images of three different regions: a) without CODs, interlayer spacing 6.85 Å; b) with CODs, interlayer spacing 6.59 Å; c) another type of CODs, interlayer spacing 6.47 Å. The arrows show adjacent layers of MnO_6 octahedra.